Supporting Information for:

Prediction of nanoparticle and colloid attachment on unfavorable mineral surfaces using representative discrete heterogeneity

Jacob Trauscht, Eddy Pazmino, and William P. Johnson[1]

Department of Geology and Geophysics, University of Utah,

Salt Lake City, Utah 84112, United States

Hamaker constants

A combined Hamaker constant (A_{132}) for interaction of CML (phase 1) with muscovite (phase 2) across water (phase 3) was obtained using the approximation below, as subscripted for the three phases (Israelachvili, 2011):

$$A_{132} \approx (\sqrt{A_{11}} - \sqrt{A_{22}})(\sqrt{A_{22}} - \sqrt{A_{33}})$$

where A_{ii} is the Hamaker constant of polystyrene, muscovite, albite, or water in vacuum. Hamaker constants for polystyrene and water in vacuum were taken from literature and were A_{22} = 6.5x10^{-20} J and A_{33} = 3.7x10^{-20} J respectively (Israelachvili, 2011). The Hamaker constant of muscovite in vacuum was averaged from three sources to yield A_{11} = 8.9x10^{-20} J (Ackler et al., 1996; Bergström, 1997; Israelachvili, 2011). Combining values:

$$A_{132} \approx \left(\sqrt{8.9x10^{-20}} - \sqrt{6.5x10^{-20}}\right)\left(\sqrt{6.5x10^{-20}} - \sqrt{3.7x10^{-20}}\right) = 2.72x10^{-21}$$

A Hamaker constant for albite in vacuum was not available in existing literature; however, one was calculated on the basis of Lifshitz Theory (Israelachvili, 2011):

$$A_{11} \approx \frac{3}{4} kT \left(\frac{\varepsilon_1 - \varepsilon_3}{\varepsilon_1 + \varepsilon_3}\right)^2 + \frac{3h v_e}{16\sqrt{2}} \frac{(n_1^2 - n_3^2)^2}{(n_1^2 + n_3^2)^{3/2}}$$

where k is the Boltzmann constant, T is temperature in kelvins, ε_1 is the dielectric constant of albite, ε_3 is the dielectric constant of the medium (ε_3=1 for a vacuum), h is Planck's constant, v_e is the mean electronic UV adsorption frequency for albite, n_1 is the refractive index of albite, n_3 is the refractive index of the solution (n_3=1 for vacuum). Since no electronic adsorption frequency (v_e) was available for albite, it was estimated as 3x10^{15} (1/s) based on values reported for other silicate minerals, which showed a narrow range of values from 3.2E15 (silica) and 3.0E15 (mica) (Israelachvili, 2011). The dielectric constant of albite was averaged from two sources (ε_1=6.5 ± 0.5) (Olhoeft, 1989; Rosenholtz, 1936). The refractive index of albite was averaged (n_1=1.535+/-0.004) from the three principal crystal

---

faces using the higher-end values in those ranges to reflect composition with significant anorthite end-member content in the solid solution (Deer et al., 2001). Inserting values:

$$A_{11} \approx \frac{3}{4}\left(1.38x10^{-23}\frac{m^2 kg}{s^2 K}\right)(298.15\ K)\left(\frac{6.5-1}{6.5+1}\right)^2$$

$$+ \frac{3\left(6.626x10^{-34}\frac{m^2 kg}{s}\right)(3x10^{15}s^{-1})}{16\sqrt{2}}\frac{(1.535^2-1^2)^2}{(1.535^2+1^2)^{\frac{3}{2}}} = 8.05x10^{-20}\ J$$

Inserting values yielded A_{132} for albite:

$$A_{132} \approx \left(\sqrt{8.05x10^{-20}} - \sqrt{6.5x10^{-20}}\right)\left(\sqrt{6.5x10^{-20}} - \sqrt{3.7x10^{-20}}\right)J = 1.80x10^{-21}\ J$$

Calculation of Collector Efficiency (η)

The colloid deposition rate across the area of observation (A_{obs}) was used to calculate the collector efficiency (η) via the following equation:

$$\eta = \frac{\left(\frac{\#attached}{time}\right)_{A_{OBS}}}{\left(\frac{\#injected}{time}\right)_{A_{JET}}} = \frac{\frac{\#attached}{time}}{C_o Q}$$

where C_O is the injected concentration of colloids and Q is the flow rate of the fluid that enters the cell (across the area of the jet, A_{jet}). The product C_OQ is equal to the number of particles injected per unit time across the area of the jet (A_{jet}). In simulations, colloid injection was performed across a smaller radius (R_{lim}) than R_{jet} for computational efficiency, since beyond this limiting radius (distance from the impinging jet axis) particles had zero chance of reaching the near surface fluid. An appropriate R_{lim} results in equivalent η despite increases in R_{lim} up to a limiting size where the number of colloids deposited becomes too small for accurate quantification (e.g., Pazmino 2014a). The radius of the area of observation (A_{obs}) in simulations was chosen to circumscribe the same area as the experiment-based A_{obs} (450 × 336 µm^2), and served as the exit radius in the simulations.

Maxwell Approach Implementation

Hahn and O'Melia (2004) proposed that the fraction of colloids retained in the secondary minimum

(α_{2min}) is equal to:

$$\alpha_{2min} = 1 - \int_{v_{p(hot)}}^{\infty} f_{Max}(v_p)dv_p$$

Where v_p is the particle velocity, and $f_{max(vp)}$ is the Maxwell-Boltzmann distribution cast in terms of

velocity (Kubo et al., 1966):

$$f_{Max(v_p)} = 4\pi \left(\frac{m_p}{2\pi kT}\right)^{(3/2)} v_p^2 e^{\left(\frac{-\frac{1}{2}m_p v_p^2}{kT}\right)}$$

where m_p is the particle mass, and k the Boltzmann constant and T the absolute temperature. The

integral of $f_{max(vp)}$ represents the fraction of the population of colloids with kinetic energy greater than

the corresponding secondary minimum energy depth (Φ_{2min}), where the integral lower limit is the

velocity threshold at which the colloid is "hot" enough to escape the secondary minimum:

$$v_{p(hot)} = \left(\frac{2\Phi_{2min}}{m_p}\right)^{0.5}$$

Table SI-1: Artificial Groundwater Composition (Taken from Ferris et al.,2004)

Electrolyte	Concentration (mM)
K2SO4	0.00403
MgSO4	0.448
CaCl2	1.75
NaNO3	0.0044
NaHCO3	1.10
KHCO3	0.0623

Table SI-2: Zeta potential values used in simulations where CML=carboxylate modified polystyrene latex. Values determined from measurement on a dynamic light scattering instrument.

Material	Particle Size (um)	Electrolyte	Concentration (mM)	pH	ζ-potential average (mV)	ζ-potential std. dev. (mV)
CML	0.25	NaCl	6	6.7	-35.7	4.6
CML	1.1	NaCl	6	6.7	-78.5	2.0
CML	2	NaCl	6	6.7	-79.2	0.6
CML	0.25	NaCl	20	6.7	-26	5.4
CML	1.1	NaCl	20	6.7	-48.9	5.1
CML	2	NaCl	20	6.7	-61.5	1.0
CML	0.25	NaCl	6	8	-40.8	2.9
CML	1.1	NaCl	6	8	-91	2.1
CML	2	NaCl	6	8	-80.5	1.0
CML	0.25	NaCl	20	8	-26.5	1.1
CML	1.1	NaCl	20	8	-62.2	1.3
CML	2	NaCl	20	8	-66.5	1.0
CML	0.25	$CaSO_4$	1.5	6.7	-34.9	3.3
CML	1.1	$CaSO_4$	1.5	6.7	-48.3	1.4
CML	2	$CaSO_4$	1.5	6.7	-43.7	0.5
CML	0.25	$CaSO_4$	6	6.7	-16.5	2.0
CML	1.1	$CaSO_4$	6	6.7	-32.9	0.9
CML	2	$CaSO_4$	6	6.7	-29.3	0.7
CML	0.25	AGW	1.8	6.7	-32.3	2.1
CML	1.1	AGW	1.8	6.7	-44.9	1.5
CML	2	AGW	1.8	6.7	-41.7	1.3

Table SI-3. Exemplary Simulation Parameters.

Flow and Geometry Parameters

Particle Radius	Average Jet velocity	Jet Radius	Injection Radius	Exit Radius	Chamber Height
a_p (m)	v_{jet} (m/s)	R_{jet} (m)	R_{lim} (m)	R_{exit} (m)	z_{max} (m)
1.00E-06	1.70E-03	5.00E-04	4.00E-06	2.19E-04	1.22E-03

Physical Parameters of Materials

Particle Density	Water Density	Viscosity	Temperature	Exit Radius	Chamber Height
ρ_p (kg/m^3)	ρ_w (kg/m^3)	μ (kg/m/s)	T (m)	R_{exit} (m)	z_{max} (m)
1.06E+03	9.98E+02	9.98E-04	2.98E+02	2.19E-04	1.22E-03

Colloid Elastic Parameters   **Diffusion Force Scaling Parameter**

Hysteresis Loss Factor	Young's Modulus	Multiplier of Diffusion Vector
β (kg/m^3)	K_{int} (m)	D_{fact} (-)
1.06E+03	9.98E+02	1.35E+00

van der Waals and Steric Force Parameters

Hamaker Constant	vdW Characteristic Wavelenght	Maximum Steric Repulsion	Steric Decay Length	Buffer Distance from Steric Minimum
A_{132} (J)	λ (m)	W_0 (J/m)	λ_0 (m)	d_{sep} (m)
3.84E-21	1.00E-07	2.10E-01	6.35E-11	5.00E-10

Water Chemistry and Surface Charge Parameters

Ionic Strenght	Electrolyte Valence	Collector Zeta Potential	Particle Zeta Potential
IS (mol/m^3)	z_i (-)	ζ_c (V)	ζ_p (V)
2.00E+01	1	-5.30E-02	-4.10E-02

Heterodomain Parameters   **Fluid Flow Field Parameters**

Number of Heterodomains per tile	Tile Size	Heterodomain Zeta Potential	Flow Field Coefficient 1	Flow Field Coefficient 2	Chamber Aspect Ratio Coefficeint
N_{Het} (#)	T_{size} (m)	ζ_{het} (V)	α_1 (-)	α_2 (-)	χ(-)
3.84E-21	1.50E-05	5.30E-02	-1.00E-01	6.60E-02	9.00E-01

Simulation and Time Parameters   **Ouput Settings**

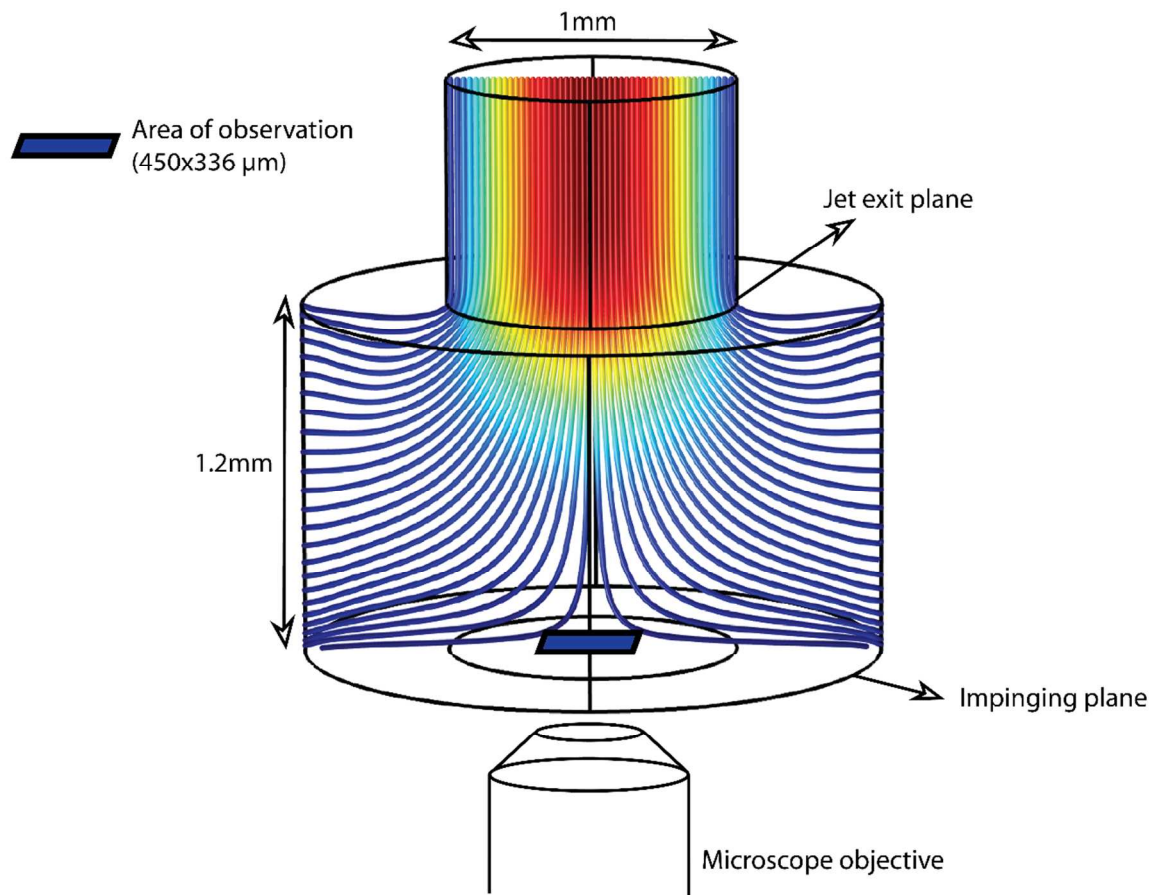| Number of Particles	Simulation Time	Multiplier of d_t for bulk trajectory	Multiplier of d_t for contact trajectory	Number of Lines of Trajectory Array	Write to Array Interval
N_{part} (#)	T_{time} (s)	MULT (-)	MULT2 (-)	N_{OUT} (#)	PI1 (#)
10000	1.00E+04	1.00E+02	1.00E+00	5000	500

Figure SI-1: Schematic of the impinging jet flow chamber. Fluid flow field is represented by color coded flow lines (red high velocity, blue low velocity). The jet is 1mm in diameter and the impinging plane is located 1.2 mm below the jet exit. Images of attached colloids are acquired via an inverted microscope across an area of observation of 450x336 µm on the impinging plane aligned with the center of the jet.
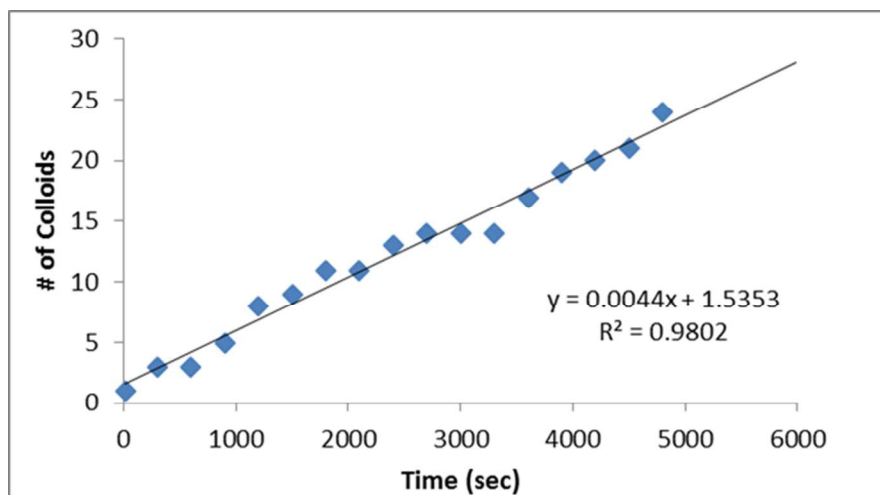
Figure SI-2. Number of colloids on surface as a function of time, experimental data from an impinging jet experiment on muscovite, 5.94×10^{-3} m/s, 6 mM, pH 6.7.
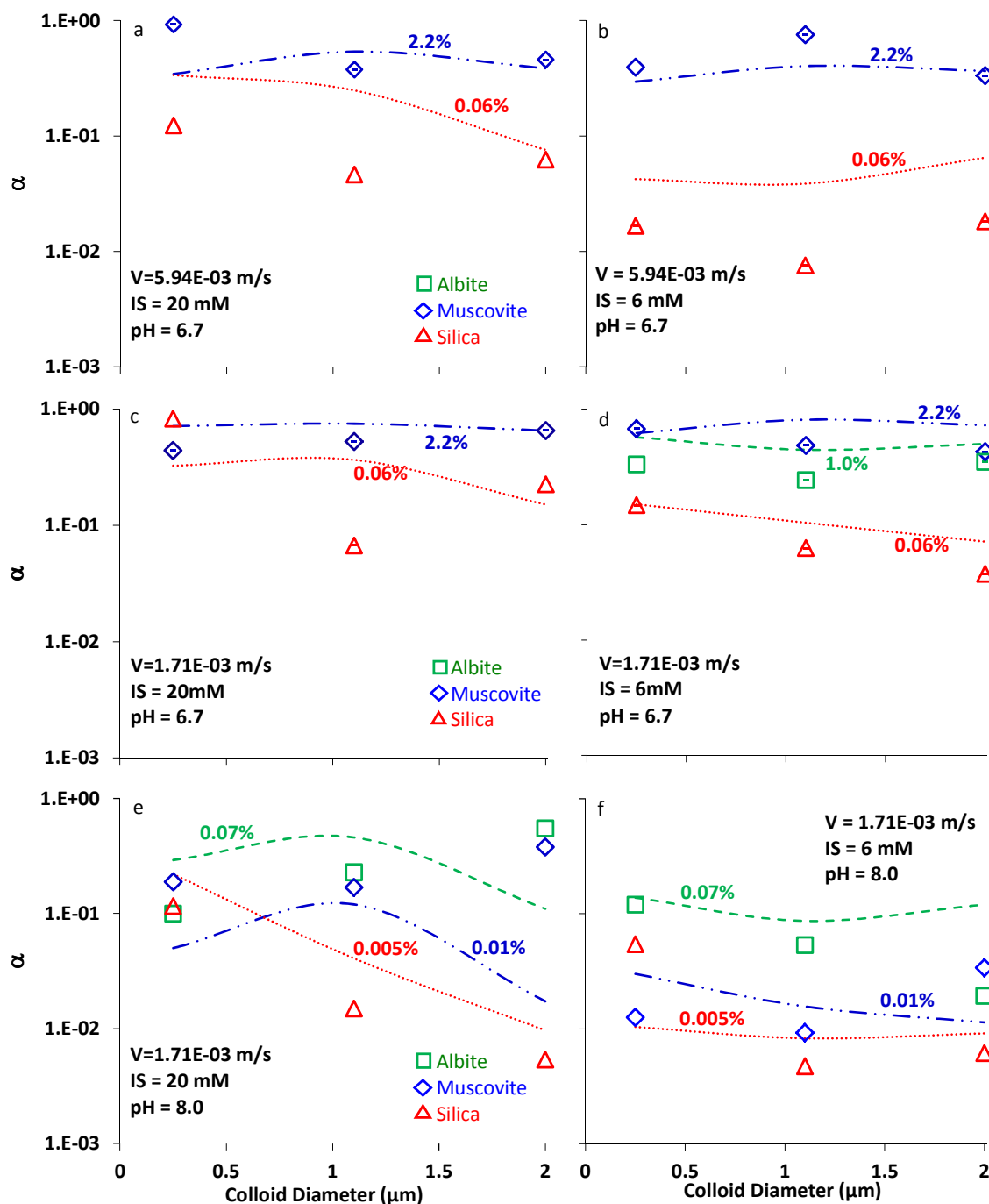
Figure SI-3. Experimentally-observed collision efficiencies (α) as a function of colloid size for soda-lime glass (red triangles), muscovite (blue diamonds) and albite (green squares) at multiple ionic strengths (6mM, 20mM), pH values (6.7 and 8.0) and fluid velocities (1.71E-03, 5.94E-03 m/s). Colored textured lines represent unfavorable condition mechanistic particle trajectory simulations (blue dash-dot=muscovite, red dot=glass, green dash=albite). A Pareto size distribution of heterodomains was approximated using a 1:4 ratio of 120 nm to 60 nm (radius) heterodomains was utilized to represent soda-lime glass collectors and muscovite and albite collectors.   Surface coverage by heterodomains is reported adjacent to simulation line.
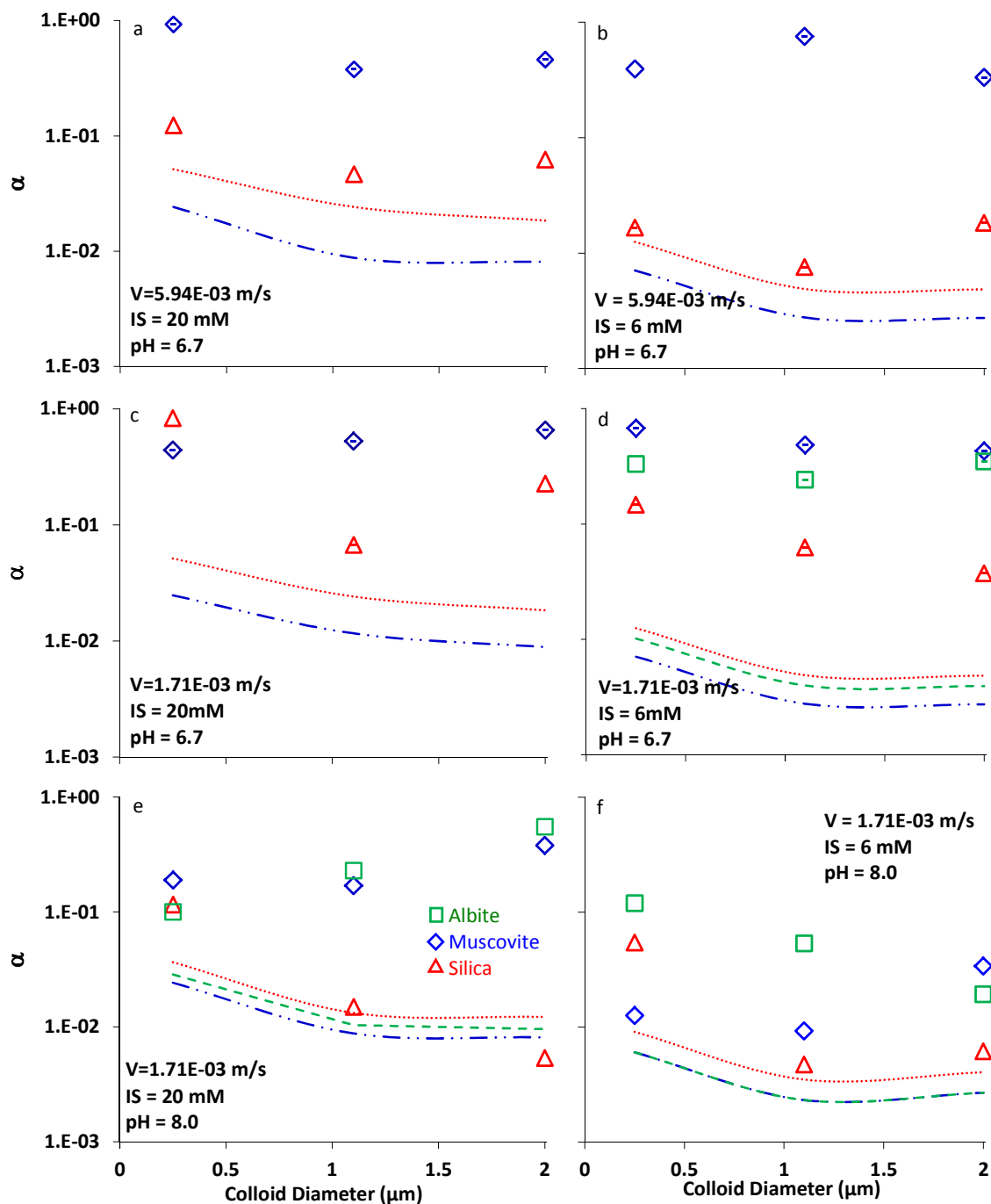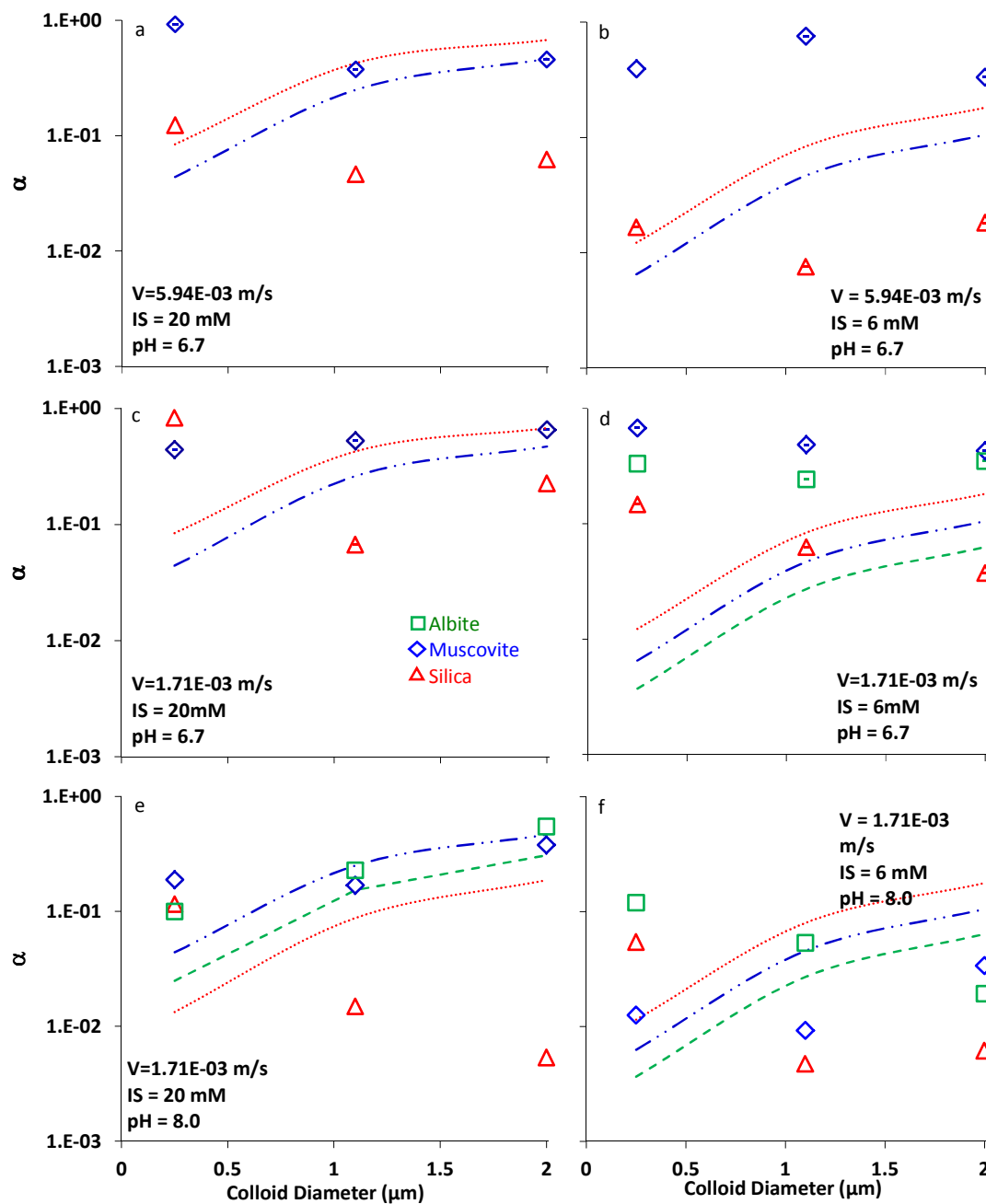
Figure SI-4: Experimentally-observed collision efficiencies (α) as a function of colloid size for soda-lime glass (red triangles), muscovite (blue diamonds) and albite (green squares) at multiple ionic strengths (6mM, 20mM), pH values (6.7 and 8.0) and fluid velocities (1.71E-03, 5.94E-03 m/s). Colored textured lines represent unfavorable condition predictions (blue dash-dot=muscovite, red dot=glass, green dash=albite). Unfavorable condition predictions were performed using the correlation equation developed by Elimelech (1992).

Figure SI-5: Experimentally-observed collision efficiencies (α) as a function of colloid size for soda-lime glass (red triangles), muscovite (blue diamonds) and albite (green squares) at multiple ionic strengths (6mM, 20mM), pH values (6.7 and 8.0) and fluid velocities (1.71E-03, 5.94E-03 m/s). Colored textured lines represent unfavorable condition predictions (blue dash-dot=muscovite, red dot=glass, green dash=albite). Unfavorable condition predictions were performed using the Maxwell approach provided by Hahn and O''Melia (2004).
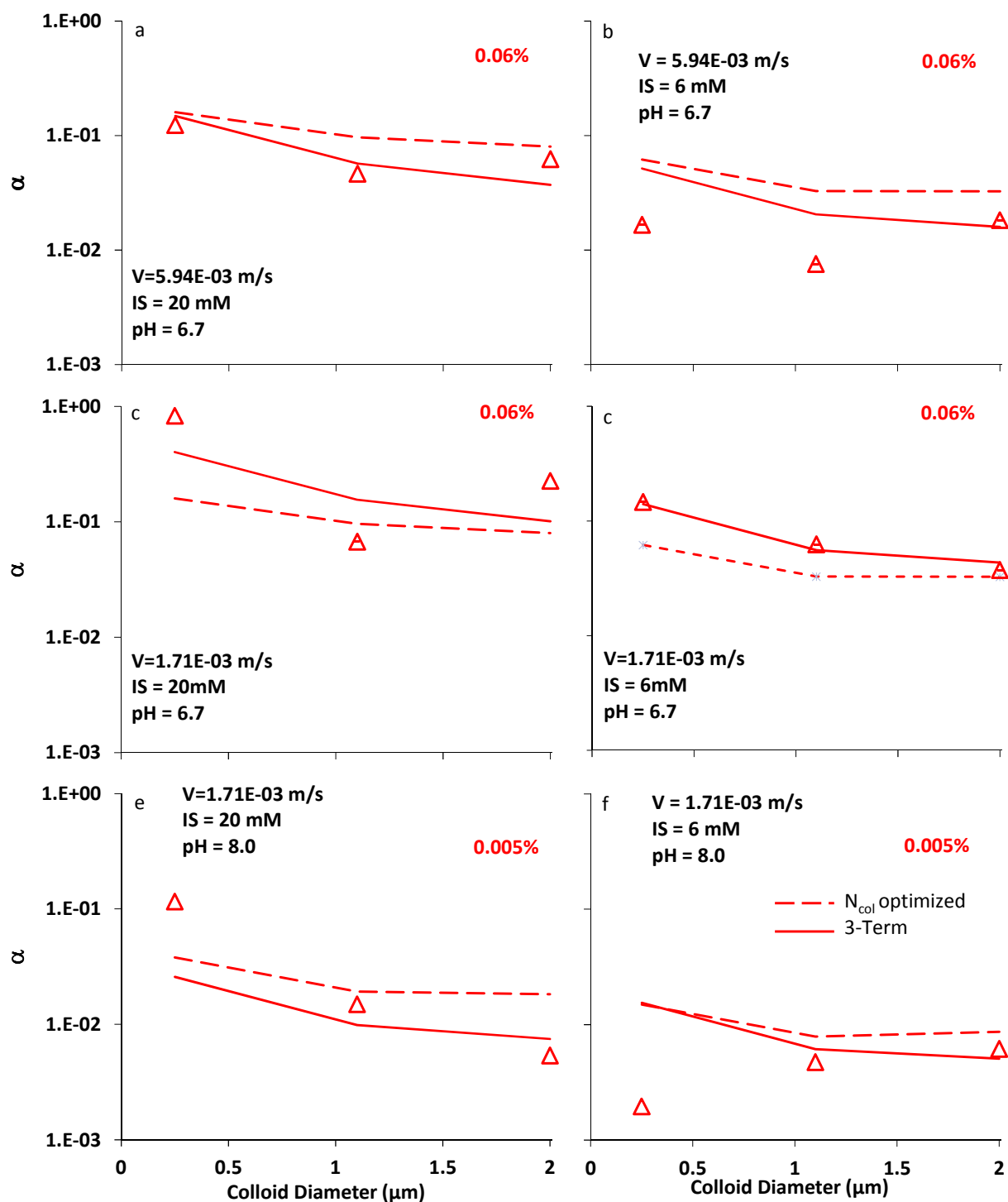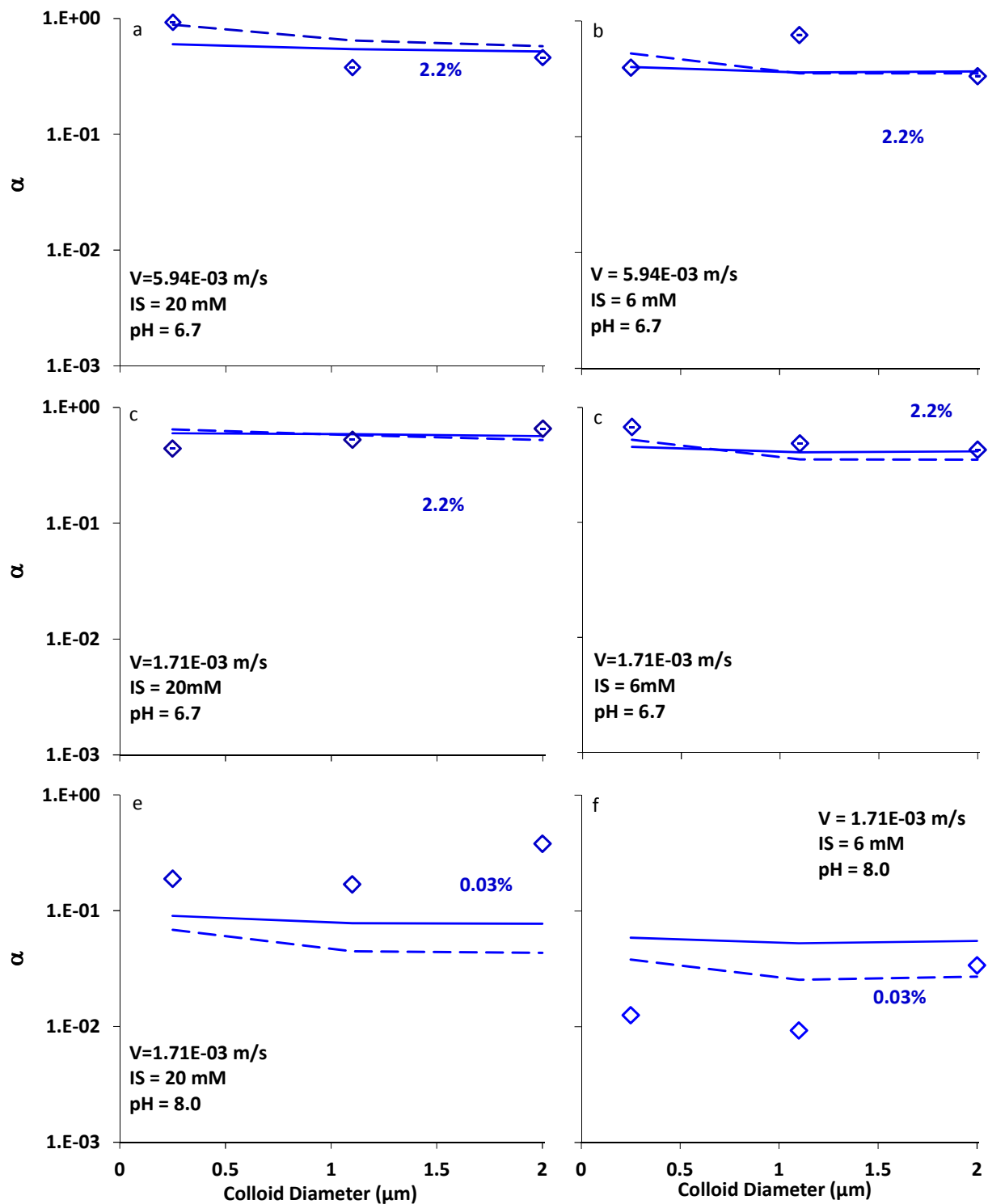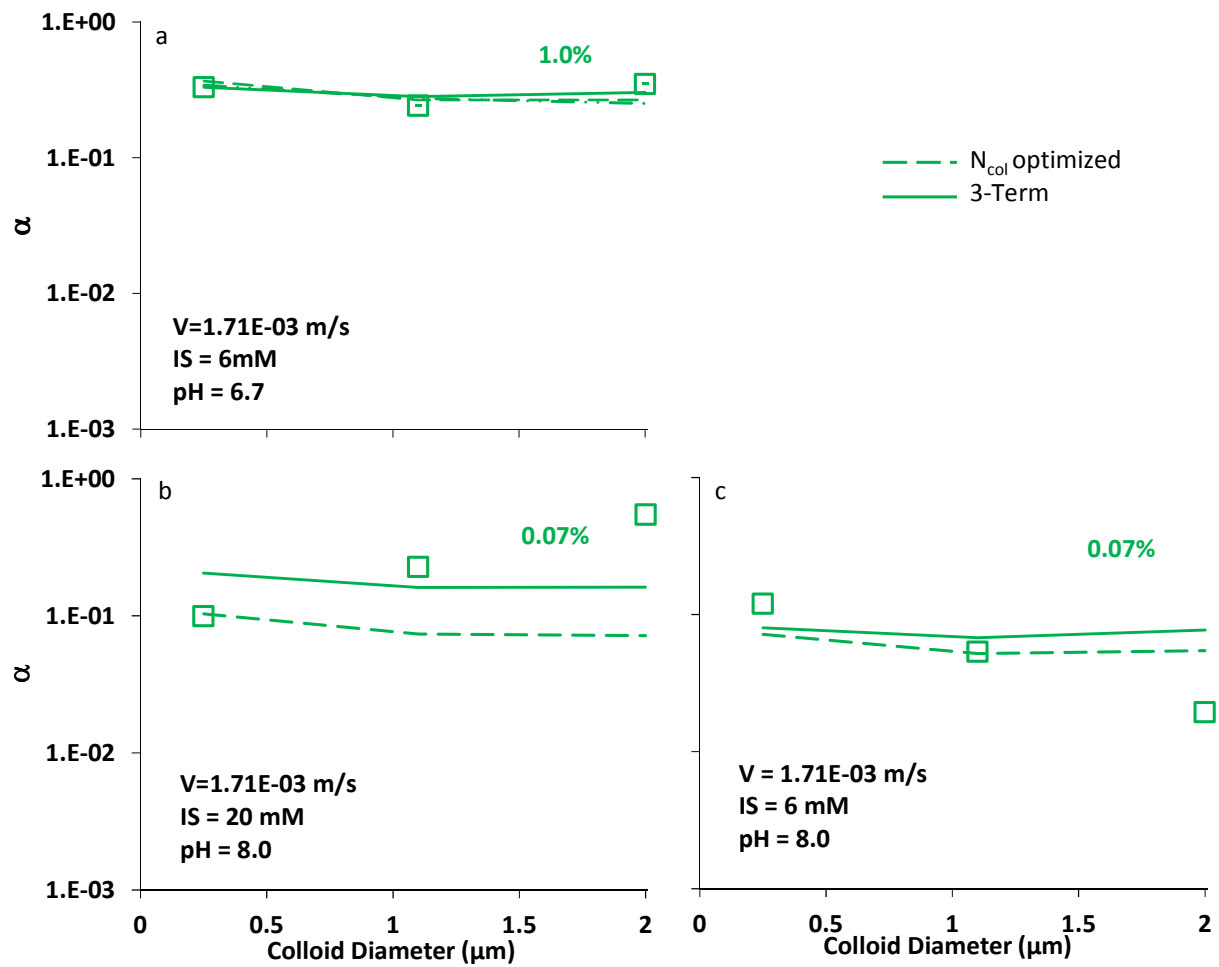
Figure SI-6: Experimentally-observed collision efficiencies (α) as a function of colloid size for soda-lime glass (symbols), at multiple ionic strengths (6mM, 20mM), pH values (6.7 and 8.0) and fluid velocities (1.71E-03, 5.94E-03 m/s). Dashed lines correspond to optimized Ncol correlation equations fit. Solid lines correspond to optimized 3-term correlation equation fit.

Figures SI-7: Experimentally-observed collision efficiencies (α) as a function of colloid size for muscovite (symbols), at multiple ionic strengths (6mM, 20mM), pH values (6.7 and 8.0) and fluid velocities (1.71E-03, 5.94E-03 m/s). Dashed lines correspond to optimized Ncol correlation equations fit. Solid lines correspond to optimized 3-term correlation equation fit.

Figures SI-8: Experimentally-observed collision efficiencies (α) as a function of colloid size for muscovite (symbols), at multiple ionic strengths (6mM, 20mM), pH values (6.7 and 8.0) and 1.71E-03 m/s fluid velocity Dashed lines correspond to optimized Ncol correlation equations fit. Solid lines correspond to optimized 3-term correlation equation fit.
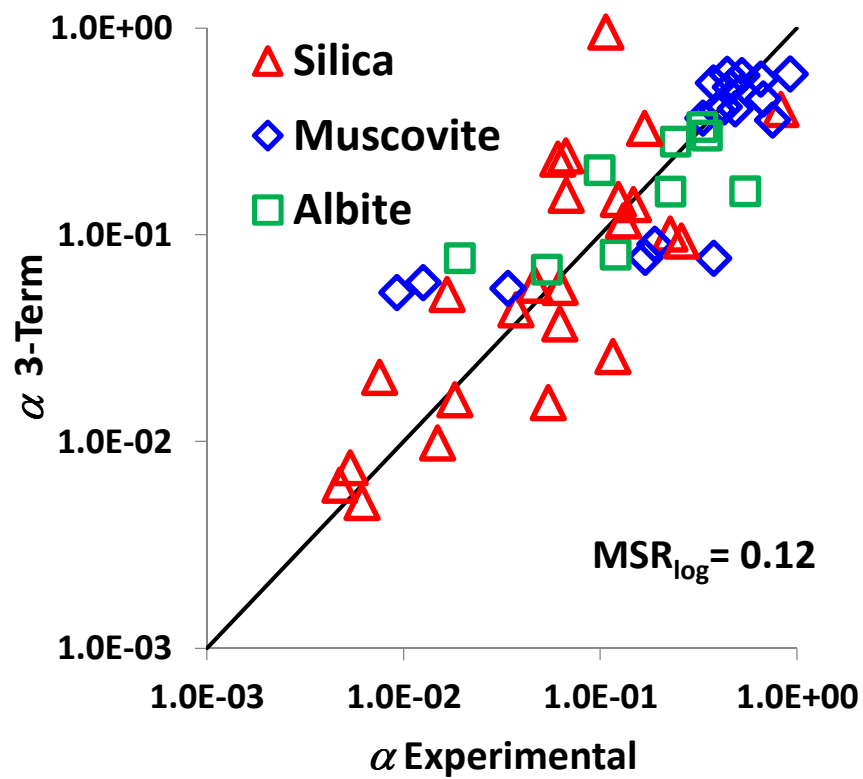
Figure SI-9: Predicted α values versus experiments (n=51) utilizing the 3-term correlation equation.

References Cited

Ackler, H. D.; French, R. H.; Chiang, Y.-M., Comparisons of Hamaker Constants for Ceramic Systems with Intervening Vacuum or Water: From Force Laws and Physical Properties. *Journal of Colloid and Interface Science* **1996,** *179* (2), 460-469.

Bergström, L., Hamaker constants of inorganic materials. *Advances in Colloid and Interface Science* **1997,** *70* (0), 125-169.

Deer, W. A.; Howie, R. A.; Zussman, J., *Rock-forming Minerals: Feldspars, Volume 4A*. Geological Society: 2001.

Hahn, M. W.; O'Melia, C. R., Deposition and Reentrainment of Brownian Particles in Porous Media under Unfavorable Chemical Conditions: Some Concepts and Applications. Environmental Science and Technology 2004, 38 (1), 210-220.

Israelachvili, J., Intermolecular and Surface Forces 3rd Edition. *Elseveier* **2011**. pp 361-370.

Kubo, R., The fluctuation-dissipation theorem. Reports on Progress in Physics 1966, 29, (1), 255.

Olhoeft, G. R., Electrical Properties of Rocks. *Physical Properties of Rocks and Minerals* **1989**.

Pazmino, E.; Trauscht, J.; Dame, B.; Johnson, W. P., Power Law Size-Distributed Heterogeneity Explains Colloid Retention on Soda Lime Glass in the Presence of Energy Barriers. *Langmuir* **2014a,** *30* (19), 5412-5421.

Rosenholtz, J. L. R. S., Dudley T., The Dielectric Constant of Mineral Powders *Rensselaer Polytechnic Institute Engineering and Science Series* **1936,** *52*.